Evaluating TERS as a Metrological Tool for the Determination of the Number of Graphene Layers at Nanoscale

Juan D. Caicedo[1,2*], Tales F.S. Dias [2], Thiago L. Vasconcelos [2] and Braulio S. Archanjo [2]

[1] Postgraduate Metrology Programme. National Institute of Metrology, Quality, and Technology, Duque de Caxias, Rio de Janeiro 25250−020, Brazil.
[2] Materials Metrology Division, National Institute of Metrology, Quality, and Technology, Duque de Caxias, Rio de Janeiro 25250−020, Brazil

[*]jdvasquez@colaborador.inmetro.gov.br

Abstract. This paper presents a comparative analysis of adjacent single and bilayer graphene samples using micro-Raman spectroscopy and tip enhancement Raman spectroscopy (TERS) techniques. The measurements were carried out close to the diffraction limit, enabling a highly accurate characterization of the graphene layers by TERS and micro-Raman Spectroscopy. Hence, TERS experiments yield significantly improved reliability, ensuring more accurate results since it reduced the region where the number of layers are unknown from around 500 nm for micro-Raman, with 1.4 N.A. objective, to around 60 nm for TERS.

1. Introduction

Graphene is a 2D material that has been widely studied due to its unique properties and several applications [1–5]. Therefore, the ISO Technical Committee 229 and IEC Technical Committee 113 released the ISO/TS 21356-1:2021 standard to help the adaptation of graphene in the industry, which holds the potential to enhance significantly next-generation technology [6]. This standard focuses on several essential properties, including lateral size and the number of layers. To accurately measure these properties, the recommended methods are scanning electron microscopy, atomic force microscopy, and Raman analysis. In this context, Graf, Davy, et al [7] used micro-Raman to map an area with adjacent single layer graphene (SLG) and bilayer graphene (BLG) sections, comparing the intensities and position of the G and 2D bands. Schmidt U et al [8] used the combination of micro-Raman microscopy with AFM (independent) to analyse the height of graphene, intensities, and position of the G and 2D bands. However, conventional Raman spectroscopy (micro-Raman) poses a limitation, requiring flakes larger than the probe size of the instrument (typically from 500 nm to 1 μm) [9]. This limitation can be resolved with the use of TERS which combines the optical microscopy system with a scanning probe microscopy system to be capable to image, study, and broadly characterize 2D materials on scales far beyond the diffraction limit (similar in dimensions to the probe apex <30 nm) [10–13]. Despite these advantages, TERS experiments have not yet been incorporated into the ISO/TS 21356-1:2021 standard.

One area where the utilization of TERS can offer advantages is in the clusterization of the number of graphene layers on nanoscale. Rabelo et al. [14] employed TERS to examine defects in graphene nanoflakes, correlating the findings with micro-Raman measurements.

Here we applied TERS on the analyses a SLG to BLG transition in the nanoscale. The ratio between the intensities of the graphene 2D and G bands, as well as their spectral positions, was used to determine whether the sample is SLG or BLG in the so-called region of indetermination where micro-Raman is not able to differentiate them. Additionally, we present a hyperspectral image generated from the intensity of the graphene's G band and 2D band in an area smaller than the micro-Raman spot.

2. Materials and methods

Graphene was mechanically exfoliated from natural graphite and subsequently deposited onto thin glass coverslips. The confocal micro-Raman images were acquired using a Nikon inverted microscope equipped with a 60x oil immersion objective (numerical aperture: 1.4), complemented by a Helium-Neon laser ($\lambda = 632.8\,nm$). Specifically, we conducted imaging for the 2D and G bands, employing APD (Avalanche Photodiode) detection. For the 2D band, we utilized a pass band filter centered at 760 nm with a full-width half-maximum (FWHM) of 10 nm. Similarly, for the G band, we employed a slightly tilted pass band filter centered at 710 nm with a FWHM of 10 nm. The images were acquired at a size of 10 µm x 10 µm (256 x 256 pixels) with a rapid acquisition time of 10 ms. For spectral acquisition, as well as for the hyperspectral line profile, an Andor Shamrock model 303i-A equipped with a Blaze: 600 lines/mm grating was employed. The relative Raman intensity of the spectrometer was calibrated using a stable tungsten halogen light source.

The nano-Raman measurements in this study were conducted using a home-builder TERS system (the configuration has been previously described in detail in [10]). A plasmon-tunable tip pyramid (PTTP) with 30 nm of apex radio, and with the nanopyramid size of L = 475 nm in order to have its. LSPR at the tip apex adjusted to match the red laser excitation wavelength, resulting in a high spectral enhancement within the near-field (NF) region [15,16].

Subsequently, a TERS and micro-Raman hyperspectral line-profile with length of 900 nm was performed across the SLG and BLG interface. The pixel distances were set to 37,5 nm and an integration time 30 seconds for both Far Field (FF) and NF measurements. To ensure robustness and obtain reliable data, the acquisition process was repeated four times.

Finally, utilizing the TERS, we performed hyperspectral mapping over an area of 640 nm x 320 nm. A total of 2048 spectra were acquired during this mapping, with integration time of 1 second.

3. Results and discussion

This section describes measurements performed on areas with adjacent SLG and BLG, above characterized. Figure 1a shows an APD image obtained using a 2D bandpass filter. Notably, the graphene regions (highlighted by more intense areas) and the glass substrate (darker regions) are distinctly discernible. Figure 1b depicts an APD image acquired using a G bandpass filter. In addition to distinguishing between graphene and glass, the differentiation between BLG (more intense areas) and single layer graphene (less intense areas). The Raman spectrum of SLG (gray) and BLG (blue) is presented in Figure 1c. The distinction between the two can be confirmed by utilizing the I_{2D}/I_G criteria, with values of 3.2 indicating a SLG and 0.98 indicating a BLG for the incident laser wavelength used.

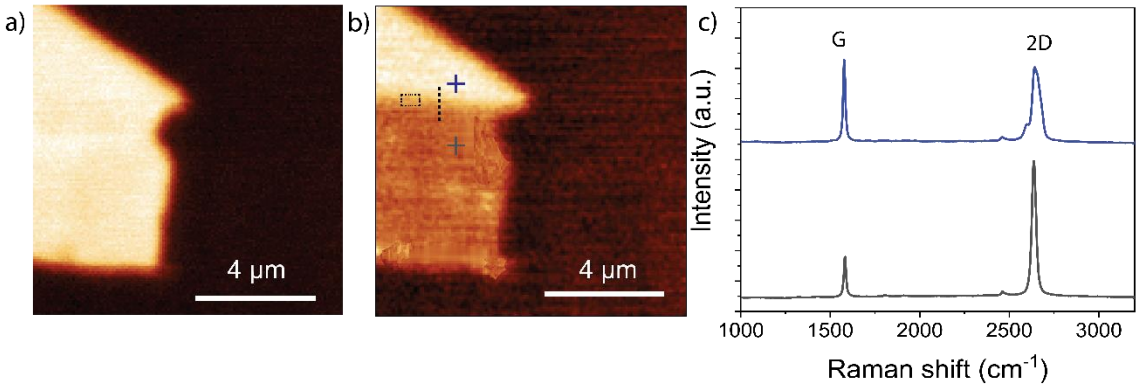

Figure 1. APD images of Graphene sample. The color scale represents the intensity of different features: a) 2D band and b) G band. c) Raman spectra of SLG and BLG associated with the graphene sample

Figure 2 presents an analysis of the spectra obtained from the hyperspectral profile acquired along the black dashed line shown in Figure 1b, for the micro-Raman (at left) and TERS (at right). Figure 2a and Figure 2b show the 2D (black) and G (blue) bands intensities. In Figure 2b, a notable variation in the intensity of the G and 2D bands is observable, indicating a characteristic behavior associated with a transition from SLG to BLG in the range of 60 nm, limited by the optical resolution of TERS in this experiment. On the contrary, Figure 2a exhibits a more gradual change, which poses a challenge in distinguishing between a SLG and a BLG. This discrepancy is attributed to the spatial resolution of TERS and micro-Raman [17,18]. Figure 2c and 2d exhibit the variation of the 2D (black) and G (blue) bands peak spectral position. In Figure 2d once again, a noticeable shift in the 2D peak position is observed, indicating a transition from a SLG to a BLG, as was observed Figure 2b. The same is not observed for G band that remains almost constant through the transition from single to bilayer graphene at micro and nano-Raman. Figure 2f displays the variation in the full width at half maximum (FWHM) of the 2D band. The observed variation, ranging from ~28 cm^{-1} to ~47 cm^{-1}, can be attributed to the transition from SLG to BLG. This deduction finds confirmation in the fact that graphene with additional layers demonstrates a FWHM greater than 60 cm^{-1} [19]. The image clearly demonstrates a significant variation behavior associated with the transition from a single layer to bilayer. On the other hand, Figure 2e illustrates a more gradual change in the FWHM of the 2D band, posing a challenge when attempting to differentiate between a SLG and a BLG structure. In all of them, the micro-Raman results remains unclear in between positions 200 nm and 780 nm, the so-called inconclusive region for FF experiments.

To confirm the observed behavior, we use a I_{2D}/I_G criteria (with confidence band) for all spectrum measured, Figure 2g and Figure 2h illustrated these criteria for micro-Raman and TERS, respectively. Clearly, in the case of TERS measurements, we can clusterize the data into three categories: SLG with a $I_{2D}/I_G > 2.2$ (highlighted area in blue), BLG graphene a $I_{2D}/I_G < 1.2$ (highlighted area in green) and a few data points that yield inconclusive results. This categorization allows for a clear distinction between SLG and BLG based on their respective I_{2D}/I_G criteria values with resolution of around 60 nm. In contrast, for micro-Raman measurement, we observed the same categories, however, at the positions in between 93 nm and 700 nm, it falls into the inconclusive category. It is important to note that the I_{2D}/I_G criteria outlined in the ISO/TS 21356-1:2021 standard are specifically defined for green laser ($\lambda = 532\ nm$) excitation and silicon subtraction. However, in this study, we employed a red excitation laser ($\lambda = 632\ nm$) and a glass substrate. Although these variations were observed, they can potentially be applied in similar cases, showcasing the efficacy of TERS. This highlights the potency of TERS as a versatile technique.

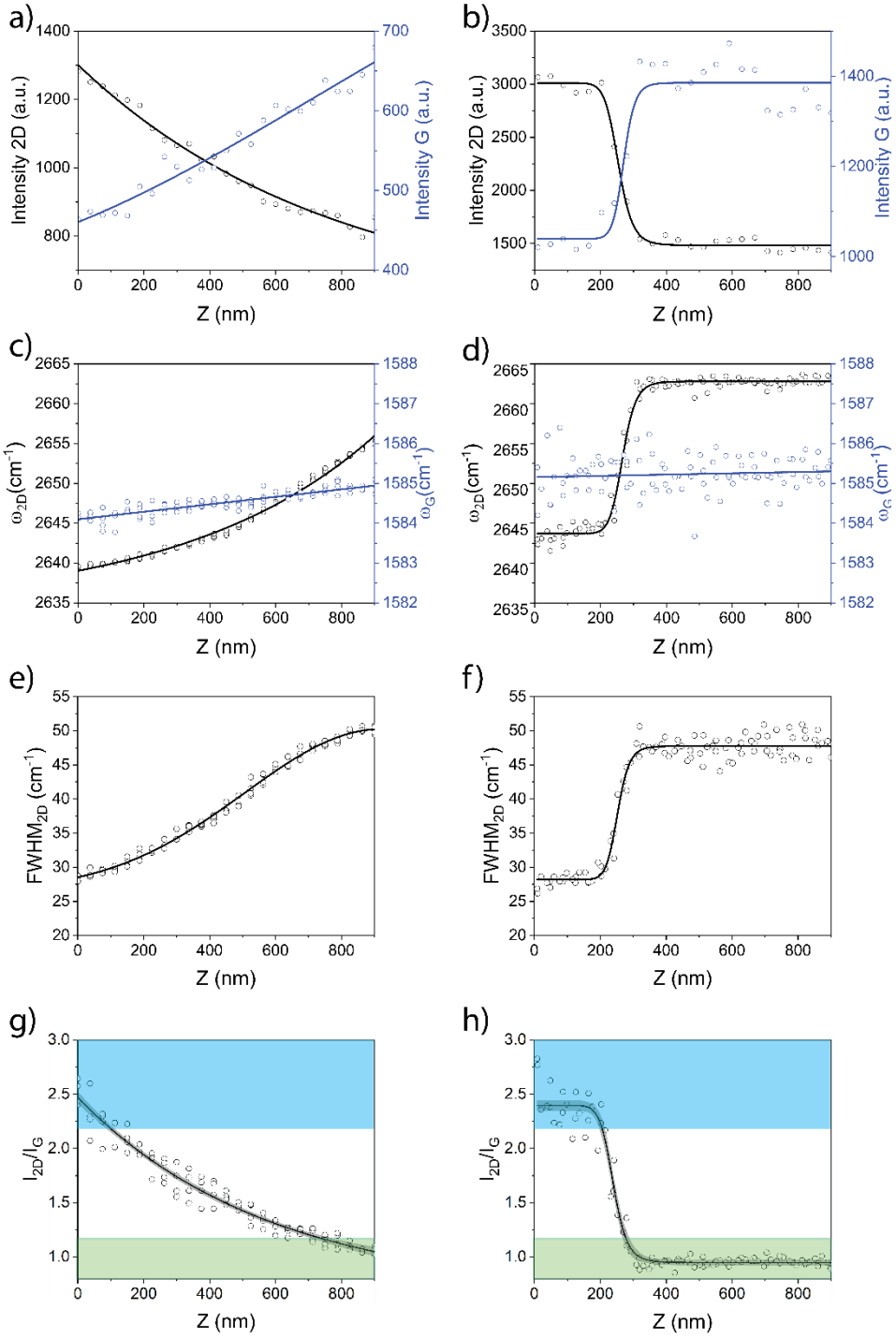

Figure 2. The first and second columns show images generated from the micro-Raman and TERS hyperspectral profile along the black dashed line in figure 1b. a) and b) intensities of the 2D band (black) and G band (blue). c) and d) spectral positions of the 2D band (black) and G band (blue). e) and f) full width at half maximum (FWHM) for the 2D band. g) and h) the I_{2D}/I_G ratio.

The fact that TERS measurements were able to cluster a greater amount of data compared to micro-Raman measurements is a clear confirmation that TERS is a better technique for the task of labelling the number of graphene layers at the Nanoscale. Moreover, we present a complete hyperspectral map of an even smaller area, in the dashed area in Figure 1b we performed a TERS experiment that presents enhancement factor of $F_{2D} = 4.1$ and $F_G = 3.2$ (measured by the ratio between spectrum acquired with PTTP and without PTTP) in SLG.

Within this specific region, TERS proved capable of distinguishing between SLG and BLG. Furthermore, by utilizing the 2D and G peak heights (Figure 3a Figure 3b) we generated images that revealed the presence of SLG, characterized by the more intense 2D peak area (and vice versa for G peak), and BLG, represented by the less intense 2D peak area (and vice versa for G peak). Then, we use the I_{2D}/I_G criteria employed in each pixel to generate Figure 3c, further confirming these findings.

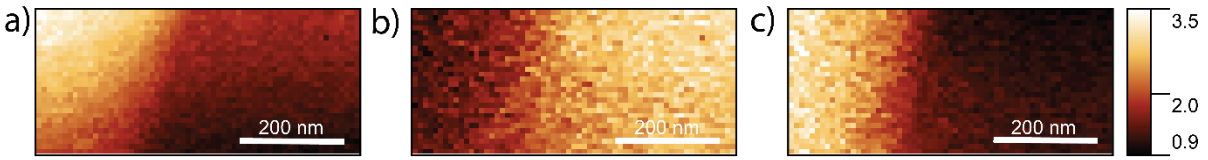

Figure 3. a), b) and c), TERS hyperspectral imaging of the square region highlighted (area of 640 nm x 320 nm) at image 1b, where the intensity renders the intensity of the 2D, G and I_{2D}/I_G ratio.

4. Conclusion

Experimental results obtained confirm the efficacy of TERS metrological tool for the characterization of SLG to BLG transitions in nanoscale. Systematic TERS measurements, utilizing the ISO/TS 21356-1:2021-1 standard's I_{2D}/I_G criteria, confirmed the capability of clusterizing SLG and BLG at the nanoscale. In contrast, the reliability of data clustering through Raman confocal measurements was found to be limited. The same measurement made by micro-Raman equipped with 1.4 N.A. objective generated an inconclusive region around 10x larger than when made by TERS.

TERS proved to be an extremely promising technique to be used as a metrological tool of practical and scientific interest for material characterization. Therefore, it is strongly advisable to undertake further comprehensive research that encompasses factors that can also changes the I_{2D}/I_G factor, what may disturb the showed criteria to distinguish SLG and BLG. For instance, the incident laser wavelength, substrate selection, method of graphene preparation and more importantly the spectrometer intensity calibration prior the measurement can have an important effect on this ratio. It is important noticing that the I_{2D}/I_G ratio is expected to be higher in TERS and dependent on tip apex size and signal enhancement as consequence of Raman coherence, as reported by Cançado et al [20]. Considering these aspects, there is significant potential for its inclusion as an alternative technique in forthcoming iterations of the ISO/TS 21356-1:2021 standard. By incorporating TERS into the standard, it would ensure that the latest advancements in material characterization are captured and provide researchers and practitioners with a comprehensive framework for accurate and reliable measurements.

References

[1] Smaisim GF, Abed AM, Al-Madhhachi H, Hadrawi SK, Al-Khateeb HMM, Kianfar E. Graphene-Based Important Carbon Structures and Nanomaterials for Energy Storage Applications as Chemical Capacitors and Supercapacitor Electrodes: a Review. Bionanoscience 2023;13:219–48. https://doi.org/10.1007/s12668-022-01048-z.

[2] Berry V. Impermeability of graphene and its applications. Carbon N Y 2013;62:1–10. https://doi.org/10.1016/j.carbon.2013.05.052.

[3] Zhao L, He R, Rim KT, Schiros T, Kim KS, Zhou H, et al. Visualizing Individual Nitrogen Dopants in Monolayer Graphene Liuyan. Science (1979) 2016;135:1–23.

[4] Zurutuza A, Marinelli C. Challenges and opportunities in graphene commercialization. Nat Nanotechnol 2014;9:730–4. https://doi.org/10.1038/nnano.2014.225.
[5] Ribeiro-Soares J, Oliveros ME, Garin C, David M V., Martins LGP, Almeida CA, et al. Structural analysis of polycrystalline graphene systems by Raman spectroscopy. Carbon N Y 2015;95:646–52. https://doi.org/10.1016/j.carbon.2015.08.020.
[6] Marciano de Oliveira Cremonezzi J, Ribeiro H, Jorge Espanhol Andrade R, José Macêdo Fechine G. Characterization strategy for graphene oxide and molybdenum disulfide: Proceedings based on the ISO/TS 21356-1:2021 standard. FlatChem 2022;36. https://doi.org/10.1016/j.flatc.2022.100448.
[7] Graf D, Molitor F, Ensslin K, Stampfer C, Jungen A, Hierold C, et al. Raman mapping of a single-layer to double-layer graphene transition. European Physical Journal: Special Topics 2007;148:171–6. https://doi.org/10.1140/epjst/e2007-00237-1.
[8] Schmidt U, Dieing T, Ibach W, Hollricher O. A Confocal Raman-AFM Study of Graphene. Micros Today 2011;19:30–3. https://doi.org/10.1017/s1551929511001192.
[9] ISO. Structural characterization of graphene. vol. 1. 2021.
[10] Rabelo C, Miranda H, Vasconcelos T, Cançado LG, Jorio A. Tip-enhanced Raman spectroscopy of graphene. 4th International Symposium on Instrumentation Systems, Circuits and Transducers (INSCIT), IEEE; 2019, p. 1–6. https://doi.org/10.1533/9780857099334.2.156.
[11] Miranda H, Rabelo C, Vasconcelos TL, Cancado LG, Jorio A. Study of the interaction between light and nanoantennas in Tip-Enhanced Raman Spectroscopy. INSCIT 2019 - 4th International Symposium on Instrumentation Systems, Circuits and Transducers 2019:1–5. https://doi.org/10.1109/INSCIT.2019.8868513.
[12] Vasconcelos TL, Archanjo BS, Oliveira BS, Silva WF, Alencar RS, Achete CA, et al. Optical Nanoantennas for Tip-Enhanced Raman Spectroscopy 2020:1–12. https://doi.org/10.1109/JSTQE.2020.3008526.
[13] Vasconcelos TL, Archanjo BS, Oliveira BS, Valaski R, Cordeiro RC, Medeiros HG, et al. Plasmon-Tunable Tip Pyramids : Monopole Nanoantennas for Near-Field Scanning Optical Microscopy 2018;1800528:1–6. https://doi.org/10.1002/adom.201800528.
[14] Rabelo C, Vasconcelos TL, Publio BC, Miranda H, Cançado LG, Jorio A. Linkage between micro- and nano-raman spectroscopy of defects in graphene. Phys Rev Appl 2020;14. https://doi.org/10.1103/PhysRevApplied.14.024056.
[15] Vasconcelos TL, Archanjo BS, Oliveira BS, Valaski R, Cordeiro RC, Medeiros HG, et al. Plasmon-Tunable Tip Pyramids: Monopole Nanoantennas for Near-Field Scanning Optical Microscopy. Adv Opt Mater 2018;6:1–6. https://doi.org/10.1002/adom.201800528.
[16] Oliveira BS, Archanjo BS, Valaski R, Achete CA, Cançado LG, Jorio A, et al. Nanofabrication of plasmon-tunable nanoantennas for tip-enhanced Raman spectroscopy. Journal of Chemical Physics 2020;153. https://doi.org/10.1063/5.0021560.
[17] Sonntag MD, Pozzi EA, Jiang N, Hersam MC, Duyne RP Van. Recent advances in tip-enhanced Raman spectroscopy probe designs. J Phys Chem Lett 2014;5:3125–30. https://doi.org/10.1007/s12274-022-5220-7.
[18] Cai ZF, Kumar N, Zenobi R. Probing On-Surface Chemistry at the Nanoscale Using Tip-Enhanced Raman Spectroscopy. CCS Chemistry 2023;5:55–71. https://doi.org/10.31635/ccschem.022.202202287.
[19] Huang M, Bakharev P V., Wang ZJ, Biswal M, Yang Z, Jin S, et al. Large-area single-crystal AB-bilayer and ABA-trilayer graphene grown on a Cu/Ni(111) foil. Nat Nanotechnol 2020;15:289–95. https://doi.org/10.1038/s41565-019-0622-8.
[20] Cançado LG, Beams R, Jorio A, Novotny L. Theory of Spatial Coherence in Near-Field Raman Scattering 2014;031054:1–14. https://doi.org/10.1103/PhysRevX.4.031054.

Acknowledgments
We acknowledge funding from the Coordenação de Aperfeiçoamento de Pessoal de Nível Superior (CAPES) and the Conselho Nacional de Desenvolvimento Científico e Tecnológico (CNPq).